Check for updates

Journal of Applied Toxicology

WILEY

Journal of AppliedToxicology

RESEARCH ARTICLE OPEN ACCESS

Liver Proteomic Alterations Induced by Chronic Fluoride Exposure in Type 2 Diabetic Mice: An Exploratory Study

Laura Ribeiro[1] | Heloisa Aparecida Barbosa da Silva Pereira[1] | Juliana Sanches Trevizol[1] | Aislan Quintiliano Delgado[2] | Aline Dionízio[1] | Tamara Teodoro Araujo[1] | Tânia Mary Cestari[1,†] | José Roberto Bosqueiro[3] | Marília Afonso Rabelo Buzalaf[1]

[1]Department of Biological Sciences, Bauru Dental School, University of São Paulo, Bauru, São Paulo, Brazil | [2]Institute of Biosciences, São Paulo State University, Botucatu, São Paulo, Brazil | [3]Department of Physical Education, Faculty of Science, São Paulo State University, Bauru, São Paulo, Brazil

Correspondence: Marília Afonso Rabelo Buzalaf (mbuzalaf@fob.usp.br)

Received: 15 May 2026 | **Revised:** 28 September 2026 | **Accepted:** 15 October 2026

Keywords: β-oxidation | fluoride | hepatic lipid metabolism | proteomics | type 2 diabetes

ABSTRACT

Water fluoridation is recognized as one of the major public health achievements of the 20th century due to its effectiveness in reducing dental caries. Recommended fluoride concentrations in drinking water (0.7–1.5 mgF/L) aim to maximize dental benefits while minimizing adverse effects. The liver plays a central role in detoxification and lipid metabolism, and recent studies suggest that fluoride exposure may disrupt lipid metabolic pathways. This exploratory study evaluated alterations in hepatic morphology, lipid profile, and liver proteome in type 2 diabetic mice chronically exposed to fluoride. Diabetic C57BL/6J mice received a high-fat diet throughout the experimental period and drinking water containing fluoride (0, 10, or 50 mgF/L) for 21 days, whereas non-diabetic control mice were maintained on a normocaloric diet with fluoride-free water. Liver fluoride levels were significantly higher in the high-dose group than in the other groups. High-dose fluoride reduced serum TG and VLDL levels compared with diabetic and nondiabetic controls, whereas low-dose fluoride increased LDL levels compared to nondiabetic controls. Hepatic glycogen content was reduced in the low-dose group. Proteomic analysis revealed overall downregulation of lipid metabolism-associated proteins in the low-dose group and upregulation of these proteins in the high-dose group. Comparison between groups showed a predominant downregulation of proteins related to mitochondrial and peroxisomal lipid oxidation. Altogether, these findings highlight a dose-dependent metabolic response to chronic fluoride exposure and suggest that fluoride may modulate lipid handling and metabolic flexibility in mice with type 2 diabetes.

1 | Introduction

Water fluoridation has been widely recognized as one of the major public health achievements of the 20th century due to its important role in reducing the global prevalence of dental caries. However, specific guidelines have been established to ensure that the benefits for oral health are maximized while limiting potential adverse effects (Buzalaf 2018). The World Health Organization (WHO) recommends a fluoride (F) concentration of 1.5 mgF/L in drinking water, whereas the American Dental Association (ADA) and the US Department of Health and Human Services recommend 0.7 mgF/L (Arakawa et al. 2009; Meenakshi et al. 2024). Following these recommendations from health agencies is essential, because exposure to elevated concentrations of F has been associated with dental and skeletal fluorosis (McDonagh 2000).

The liver plays a crucial role in detoxification of xenobiotics, including F. In addition to this function, it is a central organ in lipid metabolism, and disturbances in this process may compromise dietary lipid absorption as well as the biosynthesis

†Deceased prior to the submission of this manuscript. This publication is dedicated to her memory.

This is an open access article under the terms of the Creative Commons Attribution License, which permits use, distribution and reproduction in any medium, provided the original work is properly cited.

© 2026 The Author(s). *Journal of Applied Toxicology* published by John Wiley & Sons Ltd.

of endogenous lipids (Dionizio et al. 2019). Studies involving chronic F administration in animal models have demonstrated that this exposure can modify the expression of several proteins and enzymes involved in multiple molecular pathways across different tissues, including the liver, kidney, muscle, and heart (Barbier et al. 2010; Kobayashi et al. 2009; Leite et al. 2014; Lobo et al. 2015; Pereira et al. 2013). Elevated concentrations of F can interact with cellular systems and promote oxidative stress and lipid peroxidation (Barbier et al. 2010). Moreover, previous studies have shown that animals fed a hypercaloric diet and exposed to 50 mgF/L exhibited alterations in the hepatic proteomic profile (Pereira et al. 2013) as well as reduced plasma triglyceride levels (Pereira et al. 2016).

These observations emphasize the biological relevance of F exposure especially in those receiving a hypercaloric diet. However, it is also important to investigate these effects in the context of metabolic disorders such as diabetes mellitus (DM), particularly type 2 diabetes mellitus (T2DM). According to the International Diabetes Federation (IDF), more than 500 million individuals worldwide are affected by DM (Hossain et al. 2024). DM is a metabolic disease characterized by chronic hyperglycemia, which results either from insufficient insulin production (Type 1) or from impaired responsiveness of insulin receptors (Type 2). Among these forms, T2DM is the most prevalent and is strongly influenced by genetic predisposition, diet, obesity, and sedentary lifestyle (Hossain et al. 2024; Meenakshi et al. 2024).

Considering that F exposure has been shown to modify the lipid profile in animals fed a hypercaloric diet, the present study aimed to evaluate alterations in hepatic morphology, lipid profile, and liver proteomics in T2DM mice induced by a high-fat diet, streptozotocin (STZ), and chronically exposed to drinking water with F (10 and 50 mgF/L).

2 | Material and Methods

2.1 | Animals and Experimental Procedures

All animal procedures followed the protocol previously described and established by Ribeiro et al. (2026). Experimental procedures were approved by the Institutional Animal Care and Use committee (CEEPA-FOB/USP, Protocol No. 004/2020) and conducted in compliance with the Guide for the Care and Use of Laboratory Animals (Institute of Laboratory Animal Resources, 2021). Animals were maintained under controlled conditions of temperature (22°C–24°C), relative humidity (60%), and a 12-h light/dark cycle, with free access to food and water before and after the experimental period. Animals were housed in groups of three per cage. The C57BL/6J strain was selected due to its genetic predisposition to insulin resistance and impaired glucose metabolism, characteristics that make it a widely used model for T2DM (Ribeiro et al. 2026; Srinivasan and Ramarao 2007). Male C57BL/6J mice (42 days old, $n = 10$ per group) for the diabetic experimental groups and male C57BL/6 mice (42 days old, $n = 10$) for the nondiabetic control group were obtained from the University of São Paulo. The C57BL/6J strain was selected as the T2DM model due to its well-documented genetic predisposition to insulin resistance and glucose dysregulation, whereas the C57BL/6 strain served as the normoglycemic control (Srinivasan and Ramarao 2007). This comparison was design to highlight the biological differences between healthy and diabetic phenotypes, rather than isolate the effects of F within a single genetic background. A total of 10 animals per group ($n = 10$) was selected following previous studies that adopted similar experimental protocols for diabetes and chronic F exposure, as well as in accordance with the sample size approved by the local CEEPA (Dionizio et al. 2019; Ribeiro et al. 2026; Pereira et al. 2013). After a 7-day acclimatization period under controlled conditions, C57BL/6J mice were fed a high-fat diet containing less than 1 mg/kg F, as previously described (Gilbert et al. 2011; Ribeiro et al. 2026) for at least 8 weeks, until they reached an average body weight of approximately 30 g.

After this period, T2DM was induced by intraperitoneal administration of streptozotocin (STZ; 40 mg/kg) for three consecutive days. One week after the final injection, fasting blood glucose levels were measured, and animals with values exceeding 200 mg/dL were classified as diabetic. These diabetic mice were then included in the experimental phase, during which they received F-supplemented drinking water for 21 days at concentrations of 10 mgF/L, aligned with WHO/ADA water fluoridation guidelines (human equivalent: 1–2 mgF/L), and 50 mgF/L, representative of endemic high-fluoride regions (human equivalent:

TABLE 1 | Group distribution according to each experimental condition.

Group	Experimental conditions	Water [F] (mg/L)	Human equivalent [F] (mg/L)	Exposure scenario
DC	C57BL/6J mice, high-fat diet, STZ and diabetic (> 200 mg/Dl)	0	0	Diabetic control
DF10	C57BL/6J mice, high-fat diet, STZ and diabetic (> 200 mg/Dl)	10	1–2	Diabetic (glucose> 200 mg/dL) + 1 mgF/L (aligned with WHO fluoridation guidelines)
DF50	C57BL/6J mice, high-fat diet, STZ and diabetic (> 200 mg/Dl)	50	5–10	Diabetic (glucose > 200 mg/dL) + 5 mgF/L (representing endemic F areas with elevated drinking water levels)

10991263, 0, Downloaded from https://analyticalsciencejournals.onlinelibrary.wiley.com/doi/10.1002/jat.70495 by NICE, National Institute for Health and Care Excellence, Wiley Online Library on [03/11/2026]. See the Terms and Conditions (https://onlinelibrary.wiley.com/terms-and-conditions) on Wiley Online Library for rules of use; OA articles are governed by the applicable Creative Commons License

5–10 mgF/L) (Dionizio, Araujo, et al. 2018) (see Table 1 for group allocations). Considering that F metabolism in rodents is approximately 5–10 times faster than in humans, the administered concentrations of 10 and 50 mgF/L in our animal model correspond to human-equivalent exposures of 1–2 and 5–10 mgF/L (Dunipace et al. 1995). The F concentration in the treated water was validated as previously described by (Ribeiro et al. 2026). A nondiabetic control (CND) group was included in this study. These animals shared the same housing conditions and 21-day timeline as the treated C57BL/6J mice, receiving a standard diet and fluoride-free water. Following the experimental period, the mice were euthanized via CO_2 inhalation, and plasma and liver samples were collected for subsequent analysis.

2.2 | Fluoride Quantification in Liver Tissue

F concentration in liver tissue was determined as previously described by Pereira et al. (2016). Briefly, liver samples ($n = 6$ per group) were homogenized in deionized water (200 mg/0.5 mL, 2 min), and F levels were measured following overnight HMDS-facilitated diffusion using an ion-specific electrode. Triplicate F standards (0.00475–0.95 μg F) provided >95% recovery compared to nondiffused controls. Electric potentials (mV) were converted to μg F using standard curves ($r \geq 0.99$).

2.3 | Hematoxylin and Eosin (H&E) Staining

Liver samples were fixed in 10% neutral buffered formalin, embedded in paraffin, and sectioned at a thickness of 5 μm. The tissue sections were deparaffinized in xylene, rehydrated through a graded series of ethanol (100%, 90%, and 70%) and stained with hematoxylin for 3 min. After rinsing in distilled water, the sections were counterstained with eosin for 2 min. Slides were then dehydrated through ascending ethanol concentrations (70%, 90%, and 100%) and mounted using DPX mounting medium. Histological evaluation was performed using an Axioskop 2 light microscope (Carl Zeiss Microscopy GmbH, Jena, Germany), and representative images were captured with an AxioCam HRC digital camera (Carl Zeiss Microscopy GmbH, Jena, Germany).

2.4 | Lipid Profile Assessment

2.4.1 | Total Cholesterol Quantification

Total cholesterol (TC) was measured using a colorimetric kit (K083-3, Bioclin, MG, Brazil). Plasma (2.5 μL) was mixed with 250 μL of color reagent, incubated at 37°C for 10 min, and read at 500 nm. The calibration curve included standards from 50 to 200 mg/dL, with acceptance criteria of 5% variation and $r^2 \geq 0.9$.

2.4.2 | HDL Cholesterol

HDL levels were quantified using an enzymatic assay kit (K015-1, Bioclin, MG, Brazil). Plasma (40 μL) was mixed with 40 μL of precipitating solution, vortexed for 30 s, and centrifuged at 3500 rpm for 15 min. The supernatant (10 μL) was then incubated with 100 μL of color reagent at 37°C for 10 min. Absorbance was measured at 500 nm (BioTek microplate reader). A standard curve (10–40 nmol/L) was used, and only curves with ≤5% variation and $r^2 \geq 0.9$ were accepted.

2.4.3 | LDL Cholesterol

LDL levels were estimated using the following formula, using the Friedewald equation.

$$\text{LDL} = \text{Total Cholesterol} - (\text{HDL} + \text{VLDL})$$

2.4.4 | VLDL Cholesterol

VLDL levels were estimated using the following formula using the Friedewald equation.

$$\text{VLDL} = \text{Triglycerides} \div 5$$

2.4.5 | Triglycerides

Triglyceride (TG) concentrations were determined using a monoreagent kit (K117-3, Bioclin, MG, Brazil). Plasma (2.5 μL) was added to 250 μL of reagent, incubated at 37°C for 10 min, and read at 500 nm. Calibration was performed with standards ranging from 25 to 100 mg/dL. Only curves meeting the same acceptance criteria (≤5% variation and $r^2 \geq 0.9$) were included.

2.5 | Hepatic Glycogen Analysis

Hepatic glycogen content was determined using the phenol-sulfuric acid colorimetric method. Approximately 300 mg of liver tissue ($n = 10$ per group) was incubated with 2 mL of 30% KOH and frozen. After thawing, samples were digested in a boiling water bath for 5 min, vortexed, and treated with 0.2 mL of 0.5% Na_2SO_4.Tubes were briefly returned to the boiling bath (15 s), centrifuged at 2000 rpm for 10 min at 22°C, and the supernatant was discarded. The pellet was resuspended in 2 mL of hot water, mixed, and precipitated with 6 mL of 95% ethanol. After vortexing, 3 mL of distilled water was added, and samples were incubated at 100°C for 3 min. For the assay, 500 μL of sample was diluted 1:1 with water. A glucose standard curve (10–100 mg/mL) and a water blank were prepared. To all tubes (samples, standards, and blank), 15 μL of phenol and 2 mL of concentrated sulfuric acid were added. After incubation at 100°C for 15 min, 200 μL of each reaction was transferred to a glass microplate in duplicate. Absorbance was measured at 490 nm after cooling. Calibration curves were accepted only if standard variation was ≤5% and $r^2 \geq 0.9$, ensuring method accuracy.

2.6 | Proteomics and Bioinformatics Analyses

Mouse liver tissue preserved in Hank's buffer supplemented with 10% (v/v) protease inhibitors were centrifuged at 5000×*g* for 5 min at 4°C. Each sample ($n = 6$) represents an independent biological replicate (one individual animal per group); no sample pooling was performed. The supernatant was discarded, and the resulting pellet was used for protein extraction. Proteins were extracted using a solution containing 6-M urea and 2-M thiourea

10991263, 0, Downloaded from https://analyticalsciencejournals.onlinelibrary.wiley.com/doi/10.1002/jat.70495 by NICE, National Institute for Health and Care Excellence, Wiley Online Library on [03/11/2026]. See the Terms and Conditions (https://onlinelibrary.wiley.com/terms-and-conditions) on Wiley Online Library for rules of use; OA articles are governed by the applicable Creative Commons License

in 50-mM ammonium bicarbonate buffer (pH 7.8), mixed at a 1:1 ratio. The samples were vortexed for 10 min at 4°C, followed by sonication on ice for 5 min. This was followed by two rounds of centrifugation at 20,817×*g* for 10 min at 4°C. Protein concentrations were determined using the Bradford assay. For digestion, the extracted proteins were diluted with 1.5 volumes of ammonium bicarbonate, concentrated to 150 μL, and centrifuged at 4500×*g* (4°C). Disulfide bonds were reduced with 5-mM dithiothreitol (DTT) at 37°C for 40 min and then alkylated with 10-mM iodoacetamide (IAA) in the dark for 30 min. Digestion was performed by adding trypsin (2% w/w, Thermo Scientific) and incubating overnight at 37°C. After enzymatic digestion, samples were acidified with 10 μL of 5% trifluoroacetic acid (TFA), purified and desalted using C18 Spin Columns (Thermo Scientific), and reconstituted in 3% acetonitrile and 0.1% formic acid.

Mass spectrometry analysis was carried out in technical triplicate using a Xevo G2 mass spectrometer (Waters) coupled to a nanoACQUITY UPLC system (Waters). Protein identification was performed with Protein Lynx Global Server (PLGS, v3.03), using the UniProtKB *Mus musculus* database. Statistical analysis of differential protein expression was based on a *t* test, with significance set at $p < 0.05$. Statistical significance is considered when fold change is greater than 2×. Protein–protein interaction networks were generated in the STRING database (https://string-db.org/), the organism of interest (*M. musculus*) was specified, and protein identifiers (IDs) were entered accordingly. The confidence score was set to 0.4 to balance sensitivity and specificity of predicted interactions. Gene Ontology (GO) enrichment analysis was performed using the STRING database (https://string-db.org/), focusing on the Biological Processes category. Enriched GO terms were grouped based on semantic similarity using a threshold of ≥0.8 to reduce redundancy. Results were ranked according to signal intensity, and the top 10 enriched terms were selected for visualization. Enrichment results were displayed using a mint-blue palette, with color intensity representing the strength of enrichment.

3 | Statistical Analysis

Quantitative data were tested for normality (Shapiro–Wilk) and variance homogeneity (Bartlett) to select suitable parametric or nonparametric tests. Outliers were removed using the ROUT method (false discovery rate = 5%) prior to analysis (see Tables S7–S12 for raw and excluded outliers). Nonnormally distributed variables were $\log_{10}$ transformed and, upon achieving normality, analyzed using ANOVA followed by Tukey's post hoc test. Nonnormal data were analyzed by the Kruskal–Wallis and Dunn's post hoc tests. Statistical significance was set at $p < 0.05$, using GraphPad Prism v10.0 (GraphPad Software, San Diego, CA, United States).

4 | Results

4.1 | Weight and Blood Glucose Assessment

To induce obesity and help the development of insulin resistance, animals received a high-fat diet, with body weight monitored weekly. Prior to STZ administration, no significant differences were observed among groups (mean ± SD): CND (21.20 ± 1.033 g, $n = 10$), DC (21.77 ± 1.42 g, $n = 10$), DF10 (19.81 ± 1.68 g, $n = 10$), and DF50 (19.81 ± 3.08 g, $n = 10$) (Figure S1A). Post-STZ, weights increased similarly across all groups that were diabetic and consumed the high-fat diet, with no significant differences observed between them: DC (30.57 ± 0.94 g, $n = 10$), DF10 (30.84 ± 1.03 g, $n = 10$), and DF50 (30.27 ± 0.91 g, $n = 10$). In contrast, all diabetic groups had significantly higher body weight when compared to the CND group (28.30 ± 1.9 g, $n = 10$, $p < 0.05$) (Figure S1B).

Blood glucose levels were measured 1 week before and 1 week after STZ administration. Before STZ, no significant differences were observed between groups: CND (139 ± 20.93 mg/dL, $n = 10$), DC (140 ± 18.09 mg/dL, $n = 10$), DF10 (136.2 ± 22.21 mg/dL, $n = 10$), and DF50 (128 ± 11.88 mg/dL, $n = 10$) (Figure S1C). As anticipated, STZ elevated glucose levels postinduction. At this stage, no significant differences were observed between the diabetic groups, DC (254.9 ± 41.90 mg/dL, $n = 10$), DF10 (290 ± 70.94 mg/dL, $n = 10$), and DF50 (292.4 ± 88.18 mg/dL, $n = 10$) (Figure S1D), as all animals were receiving the same high-fat diet and F-free water. The treatment with different F concentrations was only initiated after the confirmation of hyperglycemia (glycemia ≥ 200 mg/dL) in all experimental groups, which explains the statistical homogeneity of the groups following the induction. After STZ induction, all diabetic groups showed significantly higher glucose levels when compared to the CND group (138.3 ± 25.03 mg/dL, $n = 10$, $p < 0.05$) (Figure S1D).

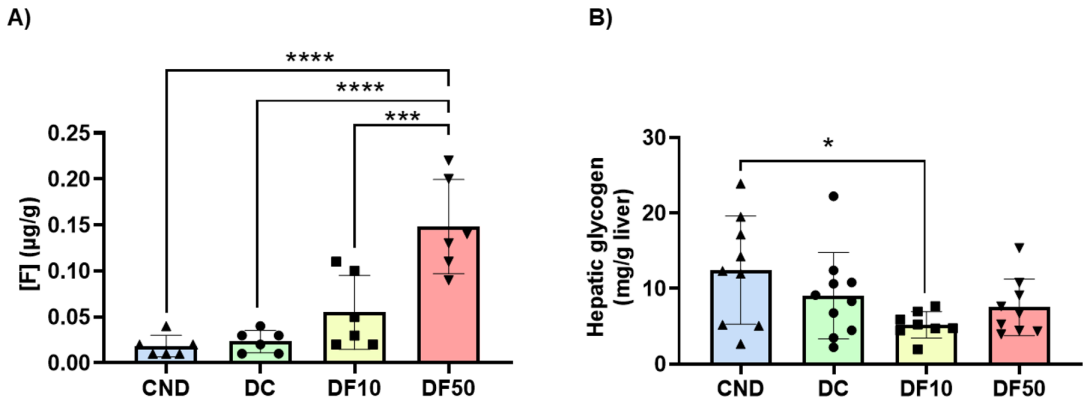

FIGURE 1 | Liver fluoride concentration and glycogen content across experimental groups and nondiabetic control. (A) Fluoride concentration (μg/g liver); (B) hepatic glycogen content (mg/g liver). Data are expressed as mean ± SD one-way ANOVA followed by Tukey's post hoc test.

10991263, 0, Downloaded from https://analyticalsciencejournals.onlinelibrary.wiley.com/doi/10.1002/jat.70495 by NICE, National Institute for Health and Care Excellence, Wiley Online Library on [03/11/2026]. See the Terms and Conditions (https://onlinelibrary.wiley.com/terms-and-conditions) on Wiley Online Library for rules of use; OA articles are governed by the applicable Creative Commons License

4.2 | Liver F Concentration

Mean (±SD) liver F levels for CND ($n = 6$), DC ($n = 6$), DF10 ($n = 6$), and DF50 ($n = 6$) were 0.018 ± 0.01 μg/g, 0.023 ± 0.01 μg/g, 0.055 ± 0.04 μg/g, and 0.148 ± 0.05 μg/g respectively. F levels in the DF50 group were significantly higher when compared with the CND, DC, and DF10 groups ($p < 0.005$; Figure 1A).

4.3 | Histological Morphological Assessment

We conducted a qualitative and exploratory descriptive histological analysis to broaden our understanding of F effects on liver architecture and morphology. Representative photomicrographs of H&E-stained liver sections were obtained at 20× and 40× magnification showing overall preservation of

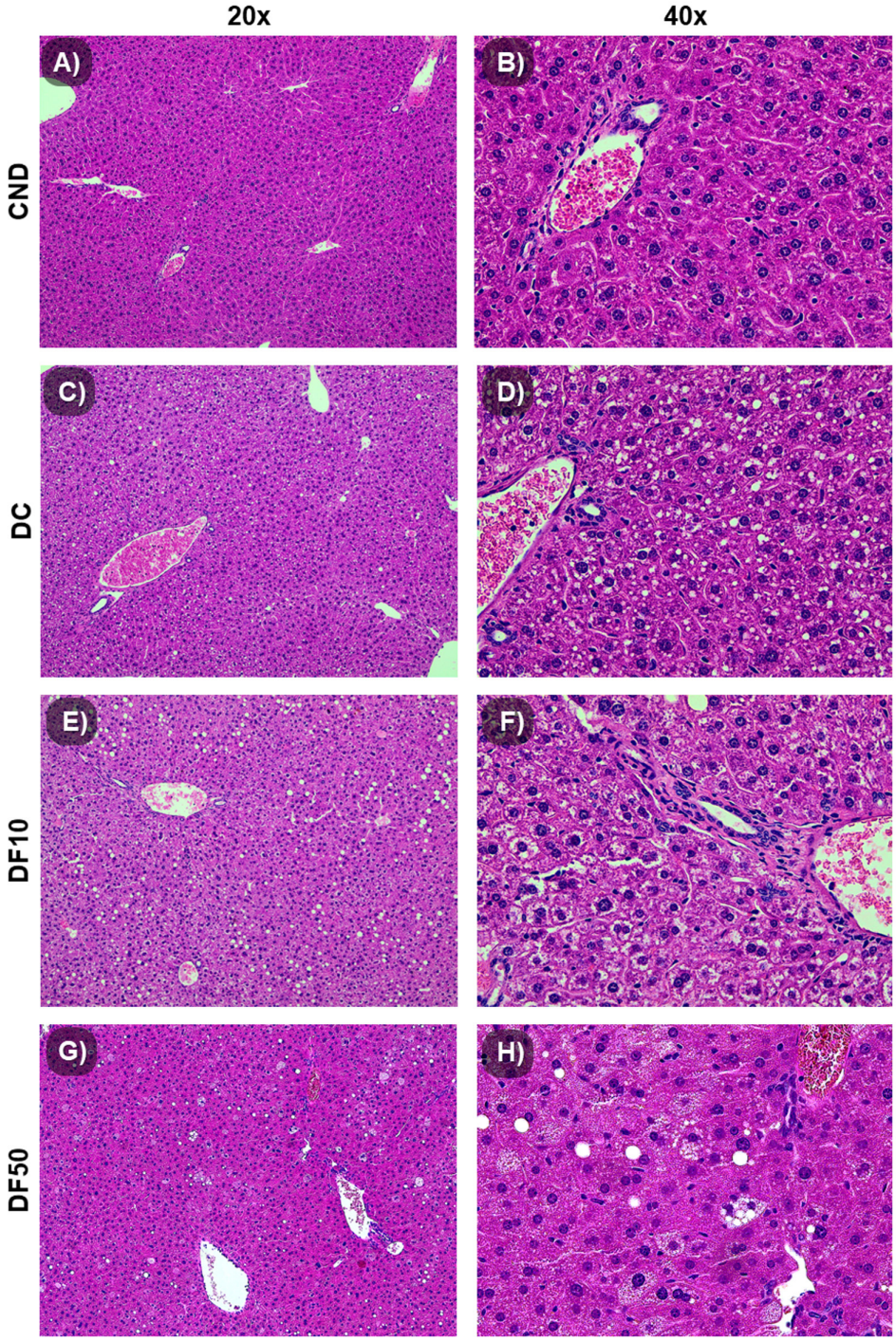

FIGURE 2 | Liver histology (H&E staining) across experimental groups and nondiabetic control. (A, B) CND group with normal lobular architecture and hepatocyte cords around the central vein; (C, D) DC group with microvesicular and macrovesicular vacuolization and inflammatory infiltrate; (E, F) DF10 group with microvesicular and macrovesicular vacuolization and inflammatory infiltrates; (G, H) DF50 group with macrovesicular vacuolization, cell swelling, and focal sinusoidal congestion. Images acquired at 20× (A, C, E, G) and 40× (B, D, F, H).

10991263, 0, Downloaded from https://analyticalsciencejournals.onlinelibrary.wiley.com/doi/10.1002/jat.70495 by NICE, National Institute for Health and Care Excellence, Wiley Online Library on [03/11/2026]. See the Terms and Conditions (https://onlinelibrary.wiley.com/terms-and-conditions) on Wiley Online Library for rules of use; OA articles are governed by the applicable Creative Commons License

the lobular architecture across all experimental groups. First, the nondiabetic control group (CND) showed normal liver histology with preserved lobular architecture, hepatocytes well-organized around the central vein, with uniform cytoplasm and free of lipid droplets. In addition, no signs of inflammatory infiltrates were observed (Figure 2A,B). In the DC group (diabetic control), the lobular architecture appeared preserved, with hepatocytes cords organized around the central vein, mild microvesicular and macrovesicular vacuolization, and discreet inflammatory infiltrates were seen (Figure 2C,D). The DF10 group exhibited a similar histological appearance to the DC group, displaying microvesicular and macrovesicular vacuolization and mild inflammatory infiltrates without signs of architectural distortion (Figure 2E,F). In contrast, the DF50 group presented larger lipid vacuoles within hepatocytes, occasional cellular swelling, and focal sinusoidal congestion. However, the portal and central vein structures remained unaffected (Figure 2G,H). These observations are purely descriptive and not representative of quantitative pathological evidence; therefore, no definitive conclusions regarding the degree of steatosis, inflammation, or fibrosis can be drawn from these data alone.

4.4 | Lipid Profile Assessment

To better investigate the effect of F on lipid metabolism in mice, plasma lipid parameters were analyzed (mean ± SD). Regarding total cholesterol (TC), no statistically significant differences were found between groups, CND (95.18 ± 17.97 mg/dL, $n = 9$), DC (109.7 ± 44.79 mg/dL, $n = 10$), DF10 (125.1 ± 28.16 mg/dL, $n = 9$), and DF50 (94.04 ± 36.75 mg/dL, $n = 10$) (Figure 3A). The same was observed for HDL, with no statistically significant differences between groups: CND (43.42 ± 4.97 mg/dL, $n = 9$), DC (33.15 ± 8.05 mg/dL, $n = 10$), DF10 (46.51 ± 20.72 mg/dL, $n = 9$), and DF50 (39.51 ± 27.31 mg/dL, $n = 10$) (Figure 3B). For the LDL analysis, the CND group (28.31 ± 30.06 mg/dL, $n = 10$) was significantly lower when compared to the DF10 group (66.57 ± 19.83 mg/dL, $n = 9$). No significant differences were observed among the remaining groups: DC (51.99 ± 36.04 mg/dL, $n = 9$), and DF50 (39.75 ± 35.03 mg/dL, $n = 10$) (Figure 3C). As for the TG analysis, the CND group (198.9 ± 66.93 mg/dL, $n = 10$) had a significantly higher value compared to the DF50 group (112.3 ± 32.15 mg/dL, $n = 9$). In addition, the DC group (200.8 ± 81.06 mg/dL, $n = 10$) also had a significantly higher value compared to the DF50 group. The remaining group, DF10 (162.2 ± 88.92 mg/dL, $n = 10$), showed no significant differences (Figure 3D). Similarly, VLDL levels were significantly higher for the CND group (39.78 ± 13.39 mg/dL, $n = 10$) compared to the DF50 group (22.46 ± 6.43 mg/dL, $n = 9$). Also, the DC group (40.15 ± 16.21 mg/dL, $n = 10$) had a significantly higher value compared to the DF50 group. The DF10 group (32.44 ± 17.79 mg/dL, $n = 10$) showed no significant differences compared to the experimental groups or the control group (Figure 3E).

4.5 | Hepatic Glycogen Assessment

Hepatic glycogen content was analyzed to further characterize the differences in glycogen storage among the experimental groups. Hepatic glycogen levels were significantly reduced in the DF10 group (5.19 ± 1.74 mg/g, $n = 8$; 2) compared to the CND group (12.4 ± 7.16 mg/g, $n = 9$; $p < 0.05$). In contrast, no significant differences were observed for the DF50 (11.45 ± 7.51 mg/g, $n = 9$) and DC groups (9.04 ± 5.73 mg/g, $n = 10$) in relation to CND, DF10, or between each other (Figure 1B).

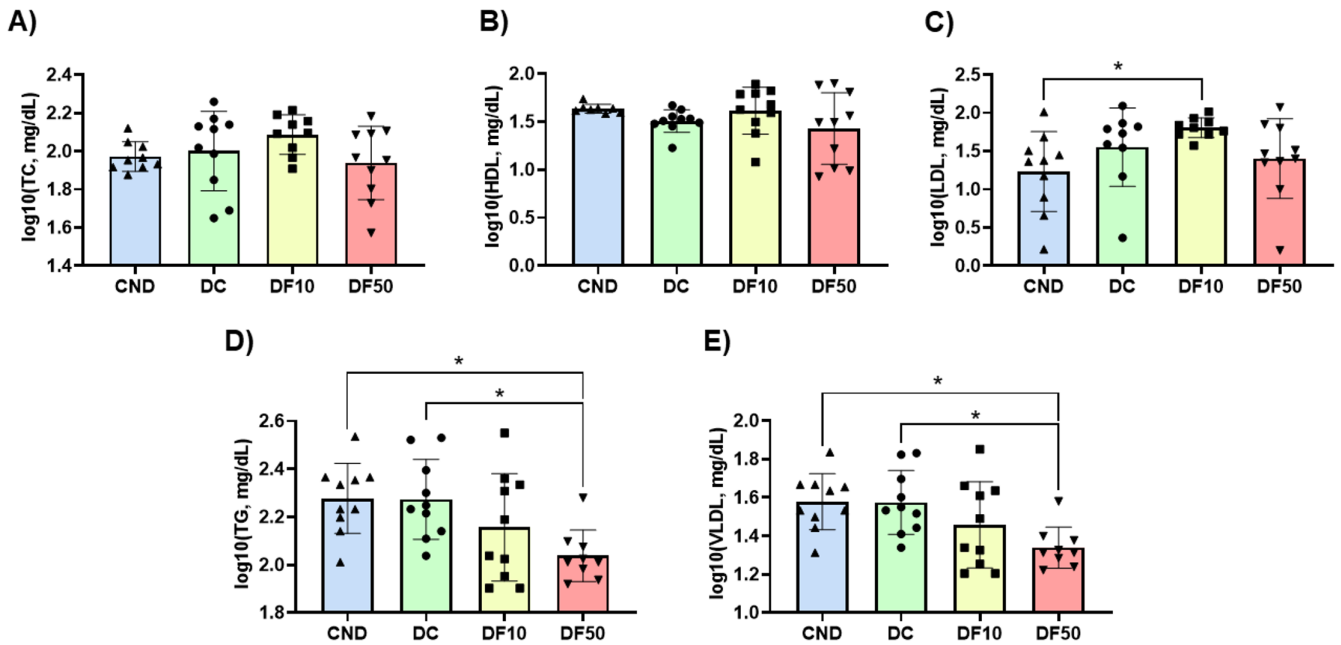

FIGURE 3 | Plasma lipid profile across experimental groups and nondiabetic control. (A) Total cholesterol (TC), (B) high-density lipoprotein (HDL), (C) low-density lipoprotein (LDL), (D) triglycerides (TG), and (E) very-low-density lipoprotein (VLDL) in CND, DC, DF10, and DF50 groups. Values are mean ± SD, expressed in $\log_{10}$mg/dL. One-way ANOVA with Tukey's test.

10991263, 0, Downloaded from https://analyticalsciencejournals.onlinelibrary.wiley.com/doi/10.1002/jat.70495 by NICE, National Institute for Health and Care Excellence, Wiley Online Library on [03/11/2026]. See the Terms and Conditions (https://onlinelibrary.wiley.com/terms-and-conditions) on Wiley Online Library for rules of use; OA articles are governed by the applicable Creative Commons License

4.6 | Proteomic Assessment

To further understand the influence of F on hepatic metabolic processes, a GO analysis focusing on biological processes was performed. First, the comparison between the DF10 and DC groups (Figure 4A) revealed that the most significantly enriched terms were carboxylic acid metabolic process and organic acid metabolic process, followed by small molecule metabolic process and carboxylic acid catabolic process. Interestingly, lipid-related pathways, including fatty acid β-oxidation as well as monocarboxylic and dicarboxylic acid metabolic processes, were also significantly enriched. The comparison between the DF50 and DC groups (Figure 4B) showed a similar enrichment profile, with most prominent terms again related to carboxylic acid, organic acid, and small molecule metabolic processes. Also, pathways associated with fatty acid metabolism, including fatty acid β-oxidation, were markedly enriched. Finally, to evaluate differences between F concentrations, the comparison between the DF50 and DF10 groups (Figure 5A) indicated that the most enriched terms were also associated with organic acid and carboxylic acid metabolic processes. In addition, enrichment of small molecule metabolism and fatty acid-related pathways, including β-oxidation, was observed. Comparison between the DC and CND groups revealed significant enrichment in small molecule catabolic process, carboxylic acid catabolic process, carboxylic acid metabolic process, and pathways related to fatty acid catabolism and beta-oxidation (Figure 5B). Enrichment analysis between DF10 versus CND revealed that the most significant terms were pathways associated with carboxylic acid metabolism, small molecule metabolism, and small molecule catabolism (Figure 6A). Comparing DF50 versus CND highlighted a significant enrichment in carboxylic acid catabolic process,

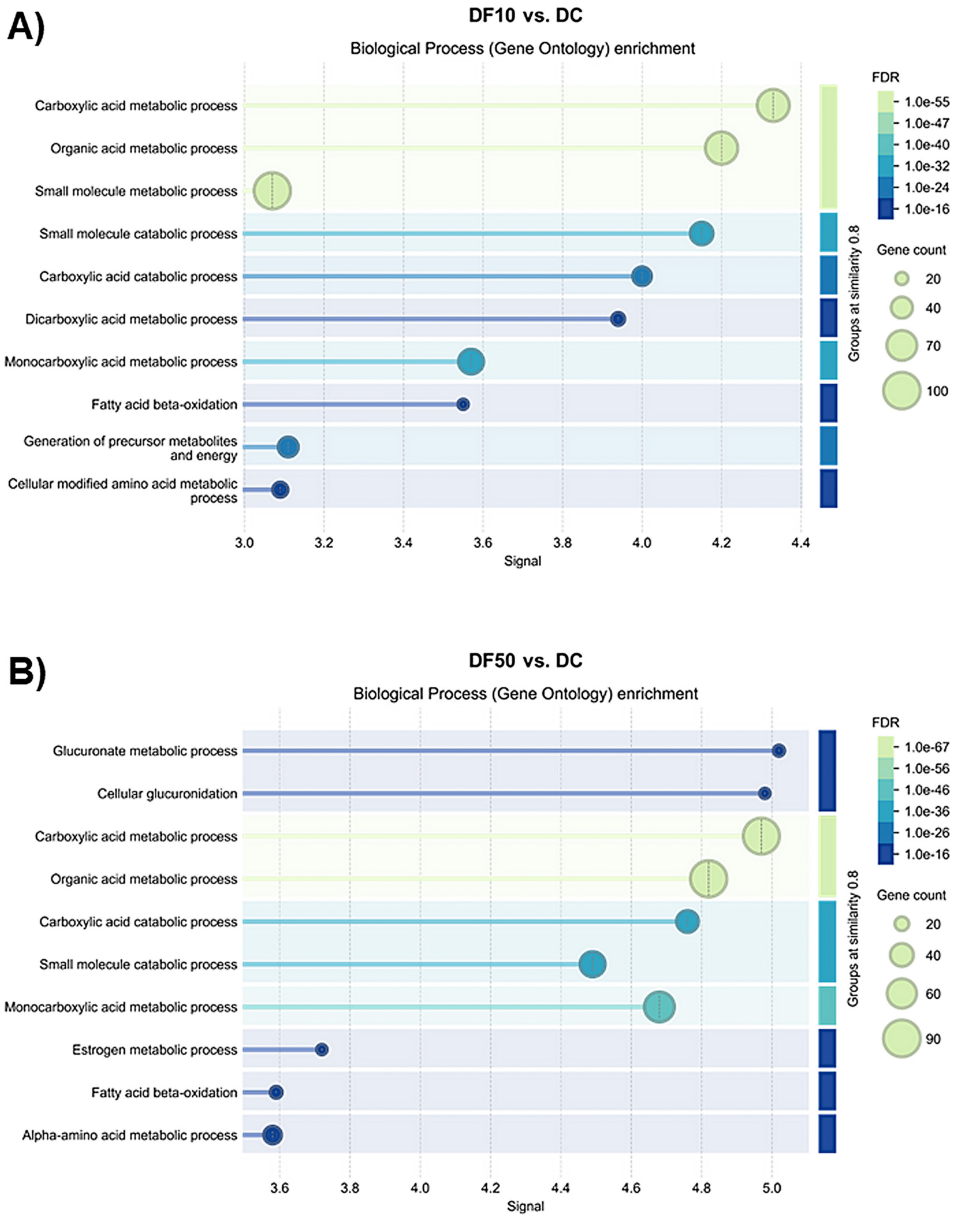

FIGURE 4 | Gene Ontology (GO) enrichment analysis of biological processes across experimental groups and nondiabetic control. (A) Comparison between DF10 and DC. (B) Comparison between DF50 and DC. The *x* axis indicates the enrichment score, and the *y* axis lists GO terms. Bubble size corresponds to the gene count, and color intensity represents the false discovery rate.

10991263, 0, Downloaded from https://analyticalsciencejournals.onlinelibrary.wiley.com/doi/10.1002/jat.70495 by NICE, National Institute for Health and Care Excellence, Wiley Online Library on [03/11/2026]. See the Terms and Conditions (https://onlinelibrary.wiley.com/terms-and-conditions) on Wiley Online Library for rules of use; OA articles are governed by the applicable Creative Commons License

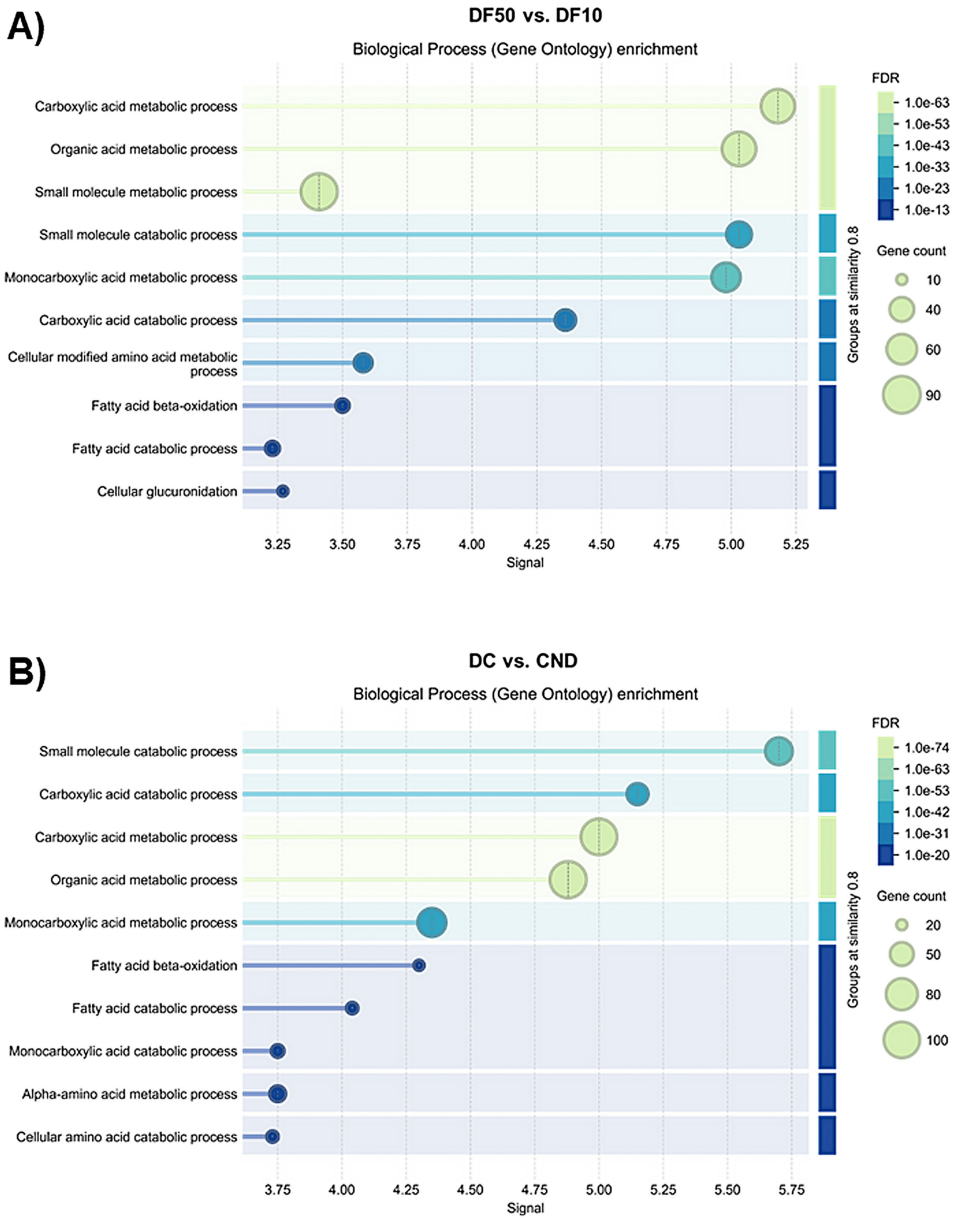

FIGURE 5 | Gene Ontology (GO) enrichment analysis of biological processes across experimental groups and nondiabetic control. (A) Comparison between DF50 and DF10. (B) Comparison between DC and CND. The *x* axis indicates the enrichment score, and the *y* axis lists GO terms. Bubble size corresponds to the gene count, and color intensity represents the false discovery rate.

small molecule catabolic process, and pathways related to fatty acid beta-oxidation and monocarboxylic acid catabolic process (Figure 6B).

Following the identification of significant alterations in lipid metabolism, specifically β-oxidation, via GO enrichment, we mapped the associated proteins into a STRING network. Protein selection was guided by UniProt functional annotations (see Tables S1–S6 for the full list of proteins identified in the proteomic analysis). The comparison between DF10 and DC revealed a plethora of downregulated proteins (Figure 7A). The most pronounced reductions were observed in enoyl-CoA isomerase (Eci1, 2.78-fold) and hydroxyacyl-coenzyme A dehydrogenase (Hadh, 2.44-fold), followed by hydroxymethylglutaryl-CoA synthase (Hmgcs2, 1.96-fold), 3-ketoacyl-CoA thiolase B (Acaa1b, 1.92-fold), 3-ketoacyl-CoA thiolase A (Acaa1a, 1.92-fold), and citrate synthase (Cs, 1.89-fold). Additionally, several proteins showed a 1.75-fold decrease, including peroxisomal acyl-coenzyme A oxidase 1 (Acox1), sterol carrier protein 2 (Scp2), and fatty acid synthase (Fasn). Finally, lower expression levels were also noted for medium-chain specific acyl-CoA dehydrogenase (Acadm, 1.41-fold), 2,4-dienoyl-CoA reductase (Decr1, 1.22-fold), long-chain specific acyl-CoA dehydrogenase (Acadl, 1.21-fold), and peroxisomal multifunctional enzyme type 2 (Hsd17b4, 1.20-fold). Regarding the comparison between DF50 and DC (Figure 7B), the analysis revealed a predominance of upregulated proteins, led by citrate synthase (Cs, 3.49-fold), acyl-CoA binding protein (Dbi, 2.97-fold), and acyl-coenzyme A synthase (Acsm1, 2.77-fold). Other significant increases were observed in enoyl-CoA synthase (Echs1, 1.97-fold), acetyl-CoA acetyltransferase (Acat2, 1.90-fold), peroxisomal bifunctional enzyme (Ehhadh,

10991263, 0, Downloaded from https://analyticalsciencejournals.onlinelibrary.wiley.com/doi/10.1002/jat.70495 by NICE, National Institute for Health and Care Excellence, Wiley Online Library on [03/11/2026]. See the Terms and Conditions (https://onlinelibrary.wiley.com/terms-and-conditions) on Wiley Online Library for rules of use; OA articles are governed by the applicable Creative Commons License

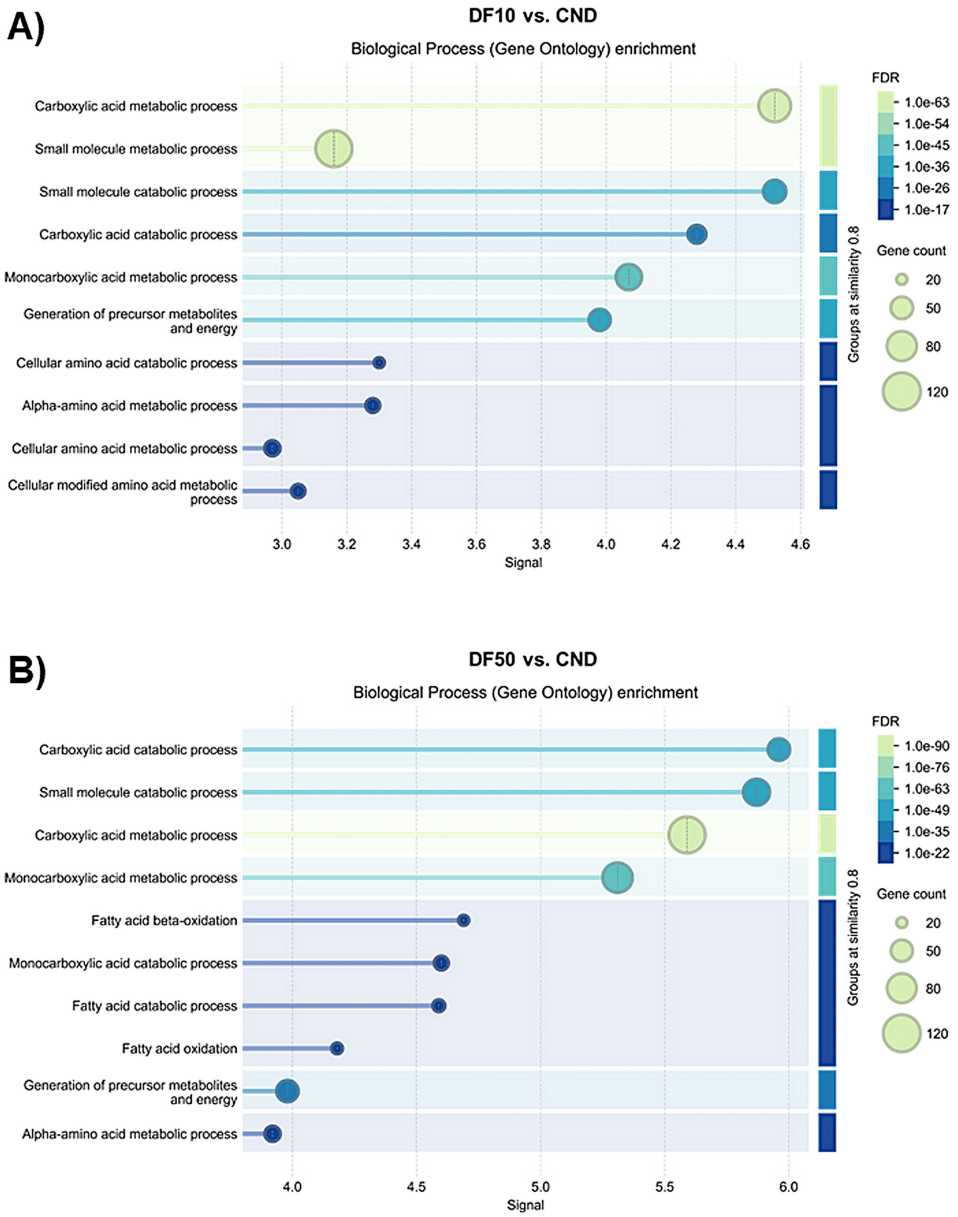

FIGURE 6 | Gene Ontology (GO) enrichment analysis of biological processes across experimental groups and nondiabetic control. (A) Comparison between DF10 and CND. (B) Comparison between DF50 and CND. The *x* axis indicates the enrichment score, and the *y* axis lists GO terms. Bubble size corresponds to the gene count, and color intensity represents the false discovery rate.

1.77-fold), and short-chain specific acyl-CoA dehydrogenase (Acads, 1.51-fold). These were followed by 3-ketoacyl-CoA thiolase A (Acaa1a, 1.48-fold), 3-ketoacyl-CoA thiolase (Acaa2, 1.34-fold), and medium-chain specific acyl-CoA dehydrogenase (Acadm, 1.31-fold). Additionally, peroxisomal multifunctional enzyme type 2 (Hsd17b4) and hydroxyacyl-CoA dehydrogenase (Hadh) both exhibited a 1.27-fold increase. Differently, electron transfer flavoprotein subunit beta (Etfb) was the only protein in this network found to be downregulated (1.18-fold). Lastly, the comparison between DF50 and DF10 (Figure 7C) showed a significant downregulation across the proteins. The most significant reduction occurred in 3-ketoacyl-CoA thiolase A (Acaa1a, 2.08-fold), followed by D-beta-hydroxybutyrate dehydrogenase (Bdh1, 1.89-fold). Decreases were also observed for enoyl-CoA hydratase (Echs1) and hydroxyacyl-CoA dehydrogenase (Hadh), both exhibiting 1.85-fold, as well as peroxisomal bifunctional enzyme (Ehhadh, 1.79-fold), fatty acid synthase (Fasn, 1.72-fold), and hydroxymethylglutaryl-CoA synthase (Hmgsc2, 1.69-fold). Other proteins showing lower expression levels included short-chain specific acyl-CoA dehydrogenase (Acads, 1.64-fold), fatty acid-binding protein (Fabp1, 1.56-fold), 2,4-dienoyl-CoA reductase (Decr1, 1.49-fold), peroxisomal acyl-CoA oxidase 1 (Acox1, 1.43-fold), and electron transfer flavoprotein subunit beta (Etfb, 1.35-fold). Finally, 3-keto-CoA thiolase (Acaa2, 1.33-fold), acetyl-CoA acetyltransferase (Acat1, 1.25-fold), and sterol carrier protein 2 (Scp2, 1.25-fold) showed the least pronounced reductions. The comparison DC versus CND revealed mostly upregulated proteins, with the highest fold changes observed for fatty acid-binding protein liver (Fabp1, 42.52-fold), nonspecific lipid-transfer protein (Scp2, 2.59-fold), hydroxymethylglutaryl-CoA synthase mitochondrial (Hmgcs2, 2.53-fold), peroxisomal 2,4-dienoyl-CoA reductase (Decr2, 2.53-fold), 3-ketoacyl-CoA

10991263, 0, Downloaded from https://analyticalsciencejournals.onlinelibrary.wiley.com/doi/10.1002/jat.70495 by NICE, National Institute for Health and Care Excellence, Wiley Online Library on [03/11/2026]. See the Terms and Conditions (https://onlinelibrary.wiley.com/terms-and-conditions) on Wiley Online Library for rules of use; OA articles are governed by the applicable Creative Commons License

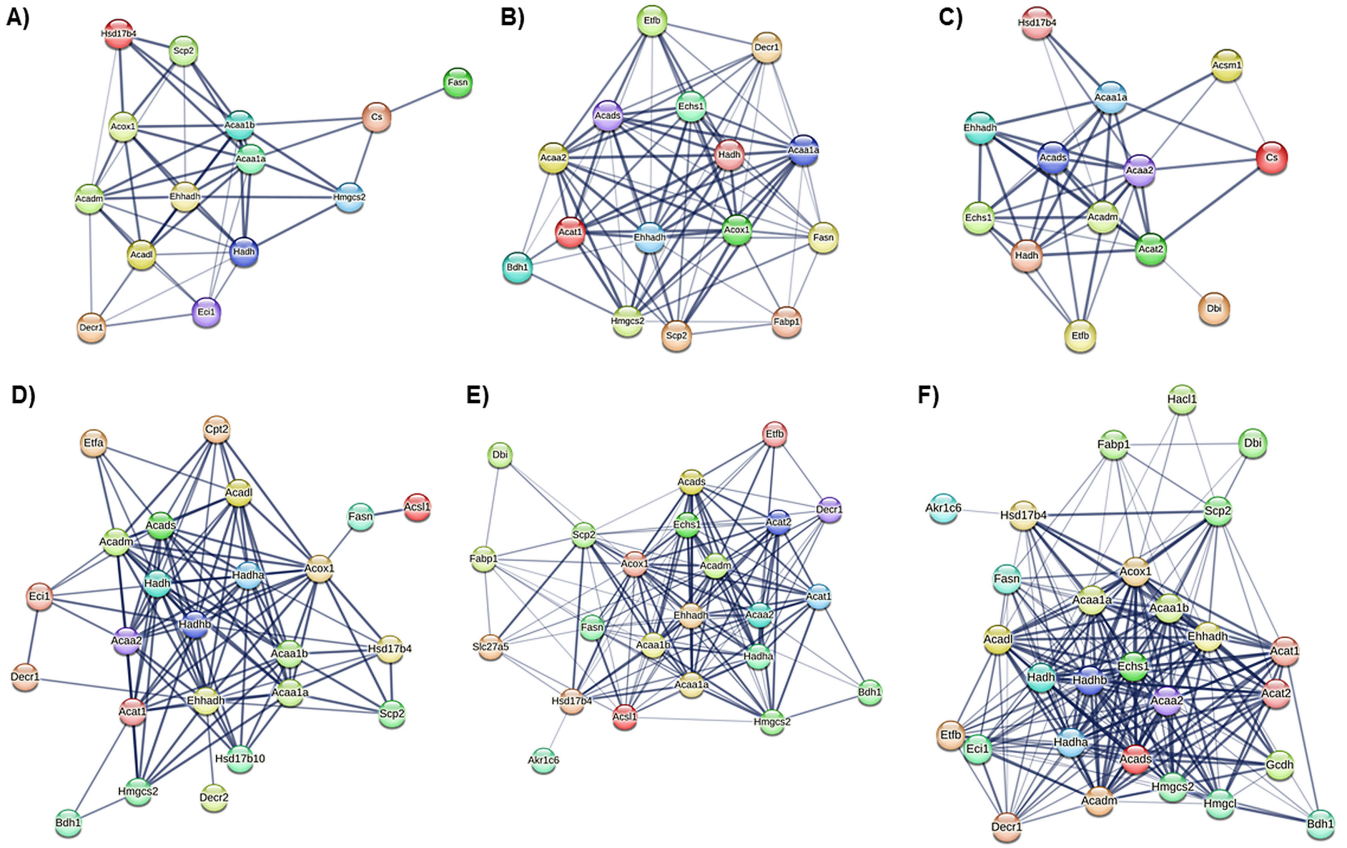

FIGURE 7 | STRING protein–protein interactions (PPI) networks of hepatic proteins associated with lipid metabolism. (A) DF10 versus DC. (B) DF50 versus DC. (C) DF50 versus DF10. (D) DC versus CND. (E) DF10 versus CND. (F) DF50 versus CND. Nodes represent proteins identified by proteomic analysis.

thiolase A peroxisomal (Acaa1a, 2.32-fold), and acetyl-CoA acetyltransferase mitochondrial (Acat1, 2.25-fold) (Figure 7D). The comparison between DF10 versus CND also revealed mostly upregulated proteins, including long-chain fatty acid transport protein 5 (Slc27a5, 5.21-fold), fatty acid-bindings protein liver (Fabp1, 4.48-fold), acetyl-CoA acetyltransferase mitochondrial (Acat1, 2.12-fold), and acetyl-CoA acetyltransferase cytosolic (Acat2, 2.08-fold) (Figure 7E). Finally, DF50 versus CND comparison showed mostly upregulated proteins, such as fatty acid-binding protein liver (Fabp1, 8.33-fold), peroxisomal bifunctional enzyme (Ehhadh, 3.53-fold), 3-ketoacyl-CoA thiolase A peroxisomal (Acaa1a, 3,42-fold), 2-hydroxyacyl-CoA lyase 1 (Hacl1, 3.42-fold), D-beta-hydroxybutyrate dehydrogenase mitochondrial (Bdh1, 3.25-fold), hydroxymethylglutaryl-CoA lyase mitochondrial (Hmgcl, 3.22-fold), and fatty acid synthase (Fasn, 3.22-fold) (Figure 7F).

5 | Discussion

The benefits of water fluoridation are undeniable, and this measure is regarded as one of the greatest public health achievements when maintained at WHO and ADA-recommended levels (Buzalaf 2018). Previous evidence from animal studies shows that chronic F consumption can alter the proteomic profile and lipid metabolism (Dionizio et al. 2019; Pereira et al. 2016). Therefore, exploratory studies aiming to further investigate the influence of chronic F treatment can be valuable, especially in the context of T2DM, a prominent metabolic disease (Meenakshi et al. 2024). In this context, this exploratory study aimed to evaluate the impact of chronic F exposure on liver morphology, lipid profile, hepatic glycogen, and the liver proteome in a T2DM mouse model. To the best of our knowledge, this is the first study to investigate the influence of F on the liver in the context of T2DM. First, to confirm the effectiveness of chronic F administration via drinking water, we measured liver F levels. As expected, the DF50 group showed the highest F accumulation among all groups. Previous studies using similar protocols observed higher F concentrations in plasma and tissues (liver, kidney, and muscle) at doses of 50 mgF/L or higher (Dionizio, Araujo, et al. 2018; Pereira et al. 2016; Trevizol et al. 2020). Additionally, exposure duration was previously shown not to alter these tissue levels (Pereira et al. 2016; Dionizio et al. 2019).

To verify the broad spectrum of F on liver morphology, histological analysis was performed using H&E staining. As the main objective was to identify potential morphological findings between the groups, the histological analysis was qualitative and exploratory. Therefore, definitive conclusions regarding the extent of hepatic steatosis cannot be drawn from these data alone. First, the nondiabetic control group (CND) showed normal liver histology with preserved lobular architecture, and no signs of inflammatory infiltrates were observed, whereas the DC and DF10 groups exhibited microvesicular and macrovesicular vacuolization and focal inflammatory infiltrates, without major

10991263, 0, Downloaded from https://analyticalsciencejournals.onlinelibrary.wiley.com/doi/10.1002/jat.70495 by NICE, National Institute for Health and Care Excellence, Wiley Online Library on [03/11/2026]. See the Terms and Conditions (https://onlinelibrary.wiley.com/terms-and-conditions) on Wiley Online Library for rules of use; OA articles are governed by the applicable Creative Commons License

lobular architecture disruption when compared to CND group. As for the DF50 group, the same microvesicular and macrovesicular vacuolization was seen, and also focal sinusoidal congestion, without major structural abnormalities. Consumption of a hypercaloric and high-fat diet is a well-established factor in the development of hepatic lipid vacuolization, and its severity is strongly associated with the duration of exposure (Dionizio, Melo, et al. 2018; Pereira et al. 2016). In the study by Pereira et al. (2016), animals fed a hypercaloric diet and exposed to 15 or 50 mgF/L for 10 or 60 days exhibited a significant reduction in hepatic lipid vacuolization only in the group treated with 50 mgF/L for 20 days. Interestingly, this effect was not sustained after 60 days, as no differences were observed among hypercaloric groups regardless of F concentration. Similarly, Dionizio et al. (2019) reported reduced hepatic lipid vacuolization in animals fed a hyper-fat diet and exposed to 50 mgF/L for 20 days. Our findings also suggest that a high-fat diet can promote the onset of lipid vacuolization; however, our morphological assessment is purely descriptive; therefore, it prevents definitive conclusions regarding the influence of chronic F exposure on the degree of the lipid vacuolization.

Moving toward a deeper understanding of the role of F in impacting metabolism, we analyzed the animals' lipid profile. Previous research indicates that F doses below 100 mgF/L administered for periods of 10–20 days significantly decrease TG levels (Dionizio, Araujo, et al. 2018; Pereira et al. 2016), whereas higher doses or longer duration can provoke the opposite effect or even show no difference (Afolabi et al. 2013; Babajko et al. 2026; Dionizio et al. 2019; Pereira et al. 2016). It has also been demonstrated that both the administered concentration and the duration of treatment are critical determinants of the observed effects (Afolabi et al. 2013; Babajko et al. 2026; Dionizio et al. 2019; Pereira et al. 2016). Our findings reinforce this dose-dependent characteristic, as it was observed a significant decrease in VLDL and TG levels in the DF50 group when compared to both CND and DC groups, which aligns with previous studies (Afolabi et al. 2013; Araujo et al. 2019; Pereira et al. 2016). Our findings in addition with previous studies could suggest that F can influence lipid metabolism, specifically those TG-rich proteins. Previous study demonstrated that chronic low-dose F exposure (10 mgF/L for 20 days) combined with a hyperlipidic diet significantly reduced LDL levels compared to control, an effect attributed to F-induced alterations in cholesterol transport pathways (Dionizio et al. 2019). In contrast, our findings revealed a significant increase in LDL levels in the DF10 group compared to the CND group. Unlike the nondiabetic model by (Dionizio et al. 2019), our study utilized a T2DM animal model. Therefore, we hypothesized that the underlying metabolic dysregulations associated with T2DM altered the physiological response to F, leading to different outcomes despite the use of similar experimental protocol.

The liver plays a central role in glycemic control by dynamically storing carbohydrates as glycogen and releasing as glucose when needed, a pathway frequently impaired in diabetes (Akatsuka et al. 1983). For this reason, hepatic glycogen content was quantified in the present study. We observed a significant reduction in glycogen content specifically in the DF10 group compared to the CND group. This finding could suggest that low-dose F can affect hepatic glycogen dynamics, potentially favoring glucose mobilization and utilization. However, whether this decrease represents a beneficial or an adverse adaptation effect remains to be further explored.

To provide a comprehensive metabolic overview, proteomic analysis was utilized as a broad-spectrum, high-sensitivity discovery tool. Regarding the results found, it is important to note that this an exploratory study, and the protein abundance changes reported here do not directly reflect enzymatic activity, metabolic flux, or functional pathway output. The results revealed a broad profile of differentially upregulated and downregulated proteins, and, through GO function analysis, significant enrichment of pathways related to fatty acids metabolism, specifically β-oxidation across all comparisons, was identified. Consequently, proteins involved in these lipid-related pathways were prioritized for further analysis, resulting in the construction of the STRING interaction networks.

In the DC versus CND comparison, an upregulation of enzymes involved in both mitochondrial and peroxisomal lipid oxidation was observed. The upregulation of peroxisomal enzymes (3-ketoacyl-CoA thiolases A and B and 2,4-dienoyl-CoA reductase) alongside mitochondrial oxidation markers reflects alterations in the lipid oxidation profile (Pereira et al. 2016; Zhang et al. 2025). The substantial increase in liver fatty acid-binding protein (42-fold) and nonspecific lipid-transfer protein may also reflect changes in the lipid-handling machinery (Huang et al. 2015). Similarly, the increase in hydroxymethylglutaryl-CoA synthase and mitochondrial acetyl-CoA acetyltransferase could indicate higher protein expression within the ketogenic pathway (Ma and Wang 2022).

Network analysis for the DF10 versus DC group revealed a significant downregulation of enzymes central to mitochondrial fatty acid degradation, such as long-chain specific Acyl-CoA dehydrogenase, hydroxyacyl-CoA dehydrogenase, and 3-ketoacyl-CoA thiolase. These enzymes are central to mitochondrial fatty acid degradation (Eaton et al. 1996; Houten and Wanders 2010). As for the DF10 versus CND comparison, the majority of proteins were upregulated in lipid metabolism and transport pathways. Long-chain fatty acid transport protein 5 exhibited the highest increase (5.21-fold). This protein catalyzes the ATP-dependent formation of fatty acyl-CoA from long-chain fatty acids and very-long-chain fatty acids (Doege et al. 2006). The upregulation of liver fatty acid-binding protein suggests impaired lipid transport in F-treated diabetic animals (Huang et al. 2015). Similarly, we observed elevated levels of both mitochondrial and cytosolic Acetyl-CoA acetyltransferase. Given that these enzymes play crucial roles in ketone body metabolism (Ma and Wang 2022), their upregulation indicates an increase in ketogenic flux in diabetic exposed to F. Although the downregulation of β-oxidation is a well-established hallmark of diabetic liver dysfunction and impaired metabolic flexibility (Koves et al. 2008), our results present a contrasting profile. Relative to diabetic control, β-oxidation proteins in the DF10 group were mostly downregulated; however, they were upregulated when compared to nondiabetic control. These proteomic findings suggest an association between low-F exposure and alterations in lipid metabolism in the context of T2DM. The distinct protein profiles observed relative to diabetic and nondiabetic controls point toward a potential shift in hepatic lipid handling, though

10991263, 0, Downloaded from https://analyticalsciencejournals.onlinelibrary.wiley.com/doi/10.1002/jat.70495 by NICE, National Institute for Health and Care Excellence, Wiley Online Library on [03/11/2026]. See the Terms and Conditions (https://onlinelibrary.wiley.com/terms-and-conditions) on Wiley Online Library for rules of use; OA articles are governed by the applicable Creative Commons License

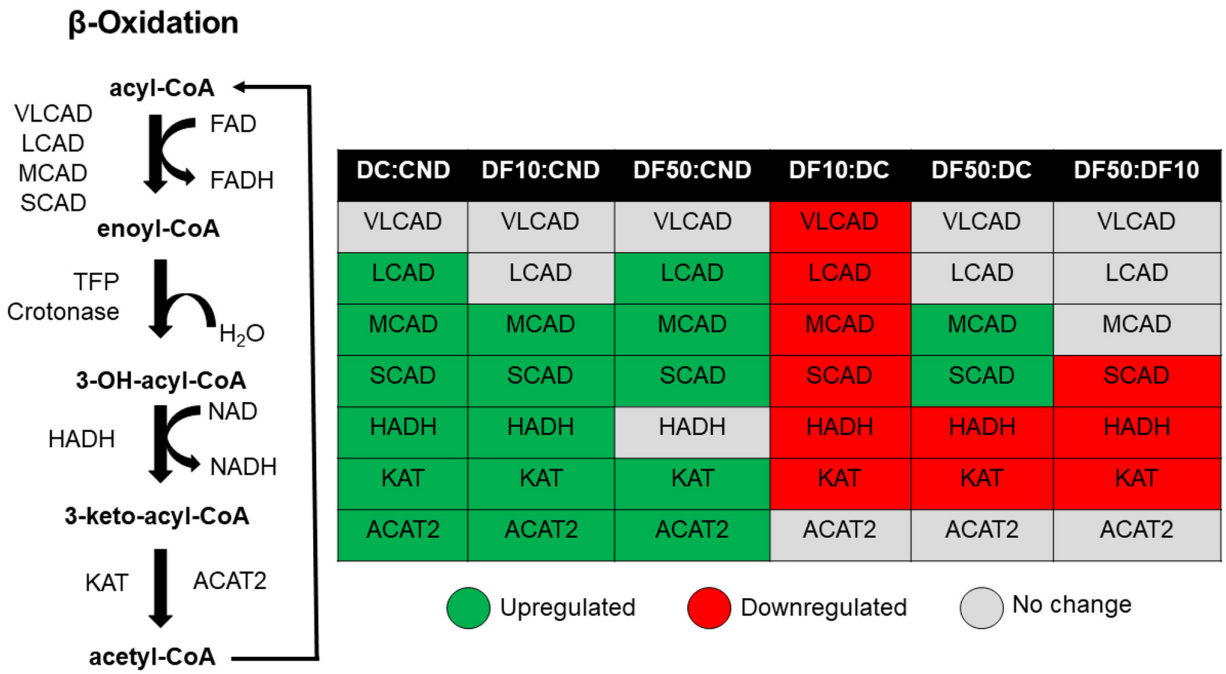

FIGURE 8 | Schematic representation of hepatic proteomic β-oxidation pathway alterations across all comparisons. Color coding indicates proteins status: red (downregulated), green (upregulated), and gray (no change) of key proteins, including very-long-chain acyl-CoA dehydrogenase (VLDL); long-chain acyl-CoA dehydrogenase (LCAD); medium-chain acyl-CoA dehydrogenase (MCAD); short-chain acyl-CoA dehydrogenase (SCAD); hydroxyacyl-CoA dehydrogenase (HADH); 3-ketoacyl-CoA thiolase (KAT); and acetyl-CoA acetyltransferase 2 (ACAT2).

whether this represents a secondary adaptation or an altered tissue response remains open to further functional studies.

In the DF50 versus DC comparison, it was observed an upregulation of key β-oxidation enzymes (such as MCAD and SCAD), consistent with previous findings regarding lipid processing proteins (Pereira et al. 2013). Our findings align with Pereira et al. (2016), who also observed a profound dysregulation of β-oxidation at 50 mgF/L. In addition, in the context of metabolic inflexibility inherent to T2DM, high abundance of these enzymes has been linked in the literature to incomplete fatty acid oxidation (Fukao et al. 2004; Koves et al. 2008). A similar pattern of mostly upregulated proteins was observed when comparing DF50 and CND. In particular, liver fatty acid-binding protein exhibited the highest increase (8.33-fold), reinforcing the observation that lipid transport proteins are elevated in both diabetic and F-treated mice, consistent with altered lipid handling. In addition, peroxisomal β-oxidation enzymes, including peroxisomal bifunctional enzyme and 3-ketoacyl-CoA thiolase A, were present upregulated, pointing to a broader shift in peroxisomal lipid pathways (Pereira et al. 2016; Zhang et al. 2025).

The DF50 versus DF10 comparison demonstrated a downregulation of enzymes involved in both mitochondrial and peroxisomal lipid oxidation. Decrease in 3-ketoacyl-CoA thiolase A, 3-ketoacyl-CoA thiolase, and related proteins points to a lower abundance of enzymes in the fatty acid oxidation pathway. Similarly, reductions in D-beta-hydroxybutyrate dehydrogenase and hydroxymethylglutaryl-CoA synthase indicate decreased protein expression within the ketogenic pathway (Zhang et al. 2025). Although F-mediated mitochondrial and oxidative impairment is recognized in the literature (Barbier et al. 2010; Pereira et al. 2013), our study highlights that the suppression of proteins within these pathways is dose-dependent in a T2DM model.

In summary, histology showed preserved architecture with lipid vacuolization across all experimental groups. Liver quantification was higher in the DF50 compared to all other groups. Regarding lipid profile, DF50 displayed lower TG and VLDL levels compared to CND and DC, whereas DF10 showed higher LDL levels compared to CND. Hepatic glycogen was significantly lower in DF10 compared to CND. Proteomically, DC versus CND revealed mostly upregulated proteins involved in mitochondrial and peroxisomal lipid oxidation. DF10 versus DC showed mostly downregulated proteins in mitochondrial fatty acid degradation, whereas DF10 versus CND showed mostly upregulated proteins related to lipid metabolism and transport. DF50 compared to both DC and CND displayed a similar pattern of upregulated proteins linked to β-oxidation. Finally, DF50 versus DF10 revealed mostly upregulated proteins in mitochondrial and peroxisomal lipid oxidation (Figure 8).

6 | Conclusion

In conclusion, this exploratory study provides insights into the impact of chronic F exposure on hepatic metabolism in a T2DM mouse model. F accumulation occurred in a dose-dependent manner. Integrated morphological, biochemical, and proteomic analyses suggest that both F dose and the diabetic condition influence hepatic lipid and glycogen metabolism. In the context of T2DM, low-dose F (10 mgF/L) was associated with reduced hepatic glycogen content and the downregulation of β-oxidation related enzymes. However, compared to nondiabetic control, it was observed mostly upregulated proteins involved

10991263, 0, Downloaded from https://analyticalsciencejournals.onlinelibrary.wiley.com/doi/10.1002/jat.70495 by NICE, National Institute for Health and Care Excellence, Wiley Online Library on [03/11/2026]. See the Terms and Conditions (https://onlinelibrary.wiley.com/terms-and-conditions) on Wiley Online Library for rules of use; OA articles are governed by the applicable Creative Commons License

in lipid metabolism and transport pathways. The high-dose F (50 mgF/L) decreased TG and VLDL levels and demonstrated mostly upregulated proteins related to β-oxidation when compared to both diabetic and nondiabetic controls, reinforcing a dose-dependent metabolic response. Altogether, these findings suggest that chronic F exposure can modulate lipid handling and metabolic flexibility in T2DM. However, given the exploratory nature of this study, our results should be interpreted as hypothesis-generating. Further studies combining functional and enzymatic assays are warranted to clarify the mechanisms underlying F-induced hepatic alterations and their implications for individuals with T2DM.

Author Contributions

Laura Ribeiro: writing – original draft, investigation, conceptualization. **Heloisa Aparecida Barbosa da Silva Pereira:** writing – review and editing, supervision, data curation. **Juliana Sanches Trevizol:** formal analysis, writing – review and editing, data curation. **Aislan Quintiliano Delgado:** formal analysis, writing – review and editing. **Aline Dionízio:** visualization, data curation. **Tamara Teodoro Araujo:** visualization, data curation. **Tânia Mary Cestari:** data curation, resources. **José Roberto Bosqueiro:** writing – review and editing. **Marília Afonso Rabelo Buzalaf:** writing – review and editing, supervision, funding acquisition.

Acknowledgments

This work was supported by the Fundação de Amparo à Pesquisa do Estado de São Paulo (FAPESP) (Proc. #2020/08138-5 and 2023/16822-1). The Article Processing Charge for the publication of this research was funded by the Coordenação de Aperfeiçoamento de Pessoal de Nível Superior - Brasil (CAPES) (ROR identifier: 00x0ma614).

Funding

This work was supported by the Fundação de Amparo à Pesquisa do Estado de São Paulo (2020/08138-5 and 2023/16822-1).

Conflicts of Interest

The authors declare no conflicts of interest.

Data Availability Statement

The data that support the findings of this study are available from the corresponding author upon reasonable request.

References

Afolabi, O. K., E. B. Oyewo, A. S. Adekunle, O. T. Adedosu, and A. L. Adedeji. 2013. "Oxidative Indices Correlate With Dyslipidemia and Pro-Inflammatory Cytokine Levels in Fluoride-Exposed Rats." *Archives of Industrial Hygiene and Toxicology* 64, no. 4: 521–529. https://doi.org/10.2478/10004-1254-64-2013-2351.

Akatsuka, A., T. J. Singh, and K.-P. Huang. 1983. "Comparison of the Liver Glycogen Synthase From Normal and Streptozotocin-Induced Diabetic Rats." *Archives of Biochemistry and Biophysics* 220, no. 2: 426–434. https://doi.org/10.1016/0003-9861(83)90432-0.

Arakawa, Y., U. K. Bhawal, T. Ikoma, et al. 2009. "Low Concentration Fluoride Stimulates Cell Motility of Epithelial Cells In Vitro." *Biomedical Research* 30, no. 5: 271–277. https://doi.org/10.2220/biomedres.30.271.

Araujo, T. T., H. A. Barbosa Silva Pereira, A. Dionizio, et al. 2019. "Changes in Energy Metabolism Induced by Fluoride: Insights From Inside the Mitochondria." *Chemosphere* 236: 124357. https://doi.org/10.1016/j.chemosphere.2019.124357.

Babajko, S., B. Marilia, F. Jean-Baptiste, and D. B. Pamela. 2026. "Water Fluoridation Risks or Benefits: Summary of the Symposium Presented During the Enamel 11 Meeting Held in Paris France." *Calcified Tissue International* 117, no. 1: 57. https://doi.org/10.1007/s00223-026-01525-7.

Barbier, O., L. Arreola-Mendoza, and L. M. del Razo. 2010. "Molecular Mechanisms of Fluoride Toxicity." *Chemico-Biological Interactions* 188, no. 2: 319–333. https://doi.org/10.1016/j.cbi.2010.07.011.

Buzalaf, M. A. R. 2018. "Review of Fluoride Intake and Appropriateness of Current Guidelines." *Advances in Dental Research* 29, no. 2: 157–166. https://doi.org/10.1177/0022034517750850.

Dionizio, A., H. A. B. S. Pereira, T. T. Araujo, et al. 2019. "Effect of Duration of Exposure to Fluoride and Type of Diet on Lipid Parameters and De Novo Lipogenesis." *Biological Trace Element Research* 190, no. 1: 157–171. https://doi.org/10.1007/s12011-018-1542-4.

Dionizio, A. S., T. T. Araujo, M. D. S. Fernandes, F. G. Iano, and M. A. R. Buzalaf. 2018. "Proposed Mechanism for Understanding the Dose- and Time-Dependency of the Effects of Fluoride in the Liver." *Toxicology and Applied Pharmacology* 358: 68–75. https://doi.org/10.1016/j.taap.2018.09.010.

Dionizio, A. S., C. G. S. Melo, I. T. Sabino-Arias, et al. 2018. "Chronic Treatment With Fluoride Affects the Jejunum: Insights From Proteomics and Enteric Innervation Analysis." *Scientific Reports* 8, no. 1: 3180. https://doi.org/10.1038/s41598-018-21533-4.

Doege, H., R. A. Baillie, A. M. Ortegon, et al. 2006. "Targeted Deletion of FATP5 Reveals Multiple Functions in Liver Metabolism: Alterations in Hepatic Lipid Homeostasis." *Gastroenterology* 130, no. 4: 1245–1258. https://doi.org/10.1053/j.gastro.2006.02.006.

Dunipace, A. J., E. J. Brizendine, W. Zhang, et al. 1995. "Effect of Aging on Animal Response to Chronic Fluoride Exposure." *Journal of Dental Research* 74, no. 1: 358–368. https://doi.org/10.1177/00220345950740011201.

Eaton, S., K. B. Bartlett, and M. Pourfarzam. 1996. "Mammalian Mitochondrial β-Oxidation." *Biochemical Journal* 320, no. 2: 345–357. https://doi.org/10.1042/bj3200345.

Fukao, T., G. D. Lopaschuk, and G. A. Mitchell. 2004. "Pathways and Control of Ketone Body Metabolism: On the Fringe of Lipid Biochemistry." *Prostaglandins, Leukotrienes and Essential Fatty Acids* 70, no. 3: 243–251. https://doi.org/10.1016/j.plefa.2003.11.001.

Gilbert, E. R., Z. Fu, and D. Liu. 2011. "Development of a Nongenetic Mouse Model of Type 2 Diabetes." *Experimental Diabetes Research* 2011: 1–12. https://doi.org/10.1155/2011/416254.

Hossain, M. J., M. Al-Mamun, and M. R. Islam. 2024. "Diabetes Mellitus, the Fastest Growing Global Public Health Concern: Early Detection Should Be Focused." *Health Science Reports* 7, no. 3: e2004. https://doi.org/10.1002/hsr2.2004.

Houten, S. M., and R. J. A. Wanders. 2010. "A General Introduction to the Biochemistry of Mitochondrial Fatty Acid β-Oxidation." *Journal of Inherited Metabolic Disease* 33, no. 5: 469–477. https://doi.org/10.1007/s10545-010-9061-2.

Huang, H., A. L. McIntosh, K. K. Landrock, et al. 2015. "Human FABP1 T94A Variant Enhances Cholesterol Uptake." *Biochimica et Biophysica Acta, Molecular and Cell Biology of Lipids* 1851, no. 7: 946–955. https://doi.org/10.1016/j.bbalip.2015.02.015.

Kobayashi, C. A. N., A. L. Leite, T. L. Silva, et al. 2009. "Proteomic Analysis of Kidney in Rats Chronically Exposed to Fluoride." *Chemico-Biological Interactions* 180, no. 2: 305–311. https://doi.org/10.1016/j.cbi.2009.03.009.

Koves, T. R., J. R. Ussher, R. C. Noland, et al. 2008. "Mitochondrial Overload and Incomplete Fatty Acid Oxidation Contribute to Skeletal

10991263, 0, Downloaded from https://analyticalsciencejournals.onlinelibrary.wiley.com/doi/10.1002/jat.70495 by NICE, National Institute for Health and Care Excellence, Wiley Online Library on [03/11/2026]. See the Terms and Conditions (https://onlinelibrary.wiley.com/terms-and-conditions) on Wiley Online Library for rules of use; OA articles are governed by the applicable Creative Commons License

Muscle Insulin Resistance." *Cell Metabolism* 7, no. 1: 45–56. https://doi.org/10.1016/j.cmet.2007.10.013.

Leite, A. L., J. Gualiume Vaz Madureira Lobo, H. A. Barbosa Da Silva Pereira, et al. 2014. "Proteomic Analysis of Gastrocnemius Muscle in Rats With Streptozotocin-Induced Diabetes and Chronically Exposed to Fluoride." *PLoS ONE* 9, no. 9: e106646. https://doi.org/10.1371/journal.pone.0106646.

Lobo, J. G. V. M., A. L. Leite, H. A. B. S. Pereira, et al. 2015. "Low-Level Fluoride Exposure Increases Insulin Sensitivity in Experimental Diabetes." *Journal of Dental Research* 94, no. 7: 990–997. https://doi.org/10.1177/0022034515581186.

Ma, X., and Q. Wang. 2022. "Short-Chain Fatty Acids Attenuate Renal Fibrosis and Enhance Autophagy of Renal Tubular Cells in Diabetic Mice Through the HDAC2/ULK1 Axis." *Endocrinology and Metabolism* 37, no. 3: 432–443. https://doi.org/10.3803/EnM.2021.1336.

McDonagh, M. S. 2000. "Systematic Review of Water Fluoridation." *BMJ* 321, no. 7265: 855–859. https://doi.org/10.1136/bmj.321.7265.855.

Meenakshi, S., T. Bahekar, P. K. Narapaka, et al. 2024. "Impact of Fluorosis on Molecular Predictors in Pathogenesis of Type 2 Diabetes Associated Microvascular Complications." *Journal of Trace Elements in Medicine and Biology* 86: 127506. https://doi.org/10.1016/j.jtemb.2024.127506.

Pereira, H. A. B. D. S., A. D. L. Leite, S. Charone, et al. 2013. "Proteomic Analysis of Liver in Rats Chronically Exposed to Fluoride." *PLoS ONE* 8, no. 9: e75343. https://doi.org/10.1371/journal.pone.0075343.

Pereira, H. A. B. S., A. S. Dionizio, M. S. Fernandes, et al. 2016. "Fluoride Intensifies Hypercaloric Diet-Induced ER Oxidative Stress and Alters Lipid Metabolism." *PLoS ONE* 11, no. 6: e0158121. https://doi.org/10.1371/journal.pone.0158121.

Ribeiro, L., H. A. B. D. S. Pereira, J. S. Trevizol, et al. 2026. "Combined Effects of Chronic High Glucose and Fluoride Exposure on Kidney Cells: Exploratory In Vitro and In Vivo Study." *Journal of Molecular Histology* 57, no. 1: 42. https://doi.org/10.1007/s10735-025-10670-6.

Srinivasan, K., and P. Ramarao. 2007. "Animal Models in Type 2 Diabetes Research: An Overview." *Indian Journal of Medical Research* 125: 451–472.

Trevizol, J. S., N. R. Buzalaf, A. Dionizio, et al. 2020. "Effects of Low-Level Fluoride Exposure on Glucose Homeostasis in Female NOD Mice." *Chemosphere* 254: 126602. https://doi.org/10.1016/j.chemosphere.2020.126602.

Zhang, Y., W. Huang, F. Huang, et al. 2025. "Fluoride Caused Injury to Endothelial Cells by Disrupting Cholesterol Synthesis." *Ecotoxicology and Environmental Safety* 305: 119160. https://doi.org/10.1016/j.ecoenv.2025.119160.

Supporting Information

Additional supporting information can be found online in the Supporting Information section. **Table S1:** List of differentially expressed proteins identified in the comparison between the DF10 vs. DC groups. The table includes the protein name, access number, PLGS score (ProteinLynx Global SERVER), and expression ratio. **Table S2:** List of differentially expressed proteins identified in the comparison between the DF50 vs. DC groups. The table includes the protein name, access number, PLGS score (ProteinLynx Global SERVER), and expression ratio. **Table S3:** List of differentially expressed proteins identified in the comparison between the DF50 vs. DF10 groups. The table includes the protein name, access number, PLGS score (ProteinLynx Global SERVER), and expression ratio. **Table S4:** List of differentially expressed proteins identified in the comparison between the DC vs. CND groups. The table includes the protein name, access number, PLGS score (ProteinLynx Global SERVER), and expression ratio. **Table S5:** List of differentially expressed proteins identified in the comparison between the DF10 vs. CND groups. The table includes the protein name, access number, PLGS score (ProteinLynx Global SERVER), and expression ratio. **Table S6:** List of differentially expressed proteins identified in the comparison between the DF50 vs. CND groups. The table includes the protein name, access number, PLGS score (ProteinLynx Global SERVER), and expression ratio. **Table S7:** Raw data obtained from hepatic glycogen assay. Numbers in red correspond to outlier values excluded from statistical analysis, identified via the ROUT test with a maximum false discovery rate set to $Q = 5\%$. **Table S8:** Raw data obtained from total cholesterol (TC) assay. Numbers in red correspond to outlier values excluded from statistical analysis, identified via the ROUT test with a maximum false discovery rate set to $Q = 5\%$. **Table S9:** Raw data obtained from HDL assay. Numbers in red correspond to outlier values excluded from statistical analysis, identified via the ROUT test with a maximum false discovery rate set to $Q = 5\%$. **Table S10:** Raw data obtained from LDL assay. Numbers in red correspond to outlier values excluded from statistical analysis, identified via the ROUT test with a maximum false discovery rate set to $Q = 5\%$. **Table S11:** Raw data obtained from TG assay. Numbers in red correspond to outlier values excluded from statistical analysis, identified via the ROUT test with a maximum false discovery rate set to $Q = 5\%$. **Table S12:** Raw data obtained from VLDL assay. Numbers in red correspond to outlier values excluded from statistical analysis, identified via the ROUT test with a maximum false discovery rate set to $Q = 5\%$. **Figure S1:** Body weight and plasma glucose across experimental groups and non-diabetic control. (A, B) Body weight (g) and (C, d) plasma glucose (mg/dL) before and after STZ induction in CND, DC, DF10, and DF50 groups. Values are mean ± SD One-way ANOVA with Tukey's test.

10991263, 0, Downloaded from https://analyticalsciencejournals.onlinelibrary.wiley.com/doi/10.1002/jat.70495 by NICE, National Institute for Health and Care Excellence, Wiley Online Library on [03/11/2026]. See the Terms and Conditions (https://onlinelibrary.wiley.com/terms-and-conditions) on Wiley Online Library for rules of use; OA articles are governed by the applicable Creative Commons License